A simple rotational spring model for laterally loaded rigid piles in sand

Wang, H.; Lehane, B. M.; Bransby, M. F.; Askarinejad, A.; Wang, L. Z.; Hong, Y.

DOI
10.1016/j.marstruc.2022.103225

Publication date
2022

Document Version
Final published version

Published in
Marine Structures

Marine Structures 84 (2022) 103225

Contents lists available at ScienceDirect

Marine Structures

journal homepage: www.elsevier.com/locate/marstruc

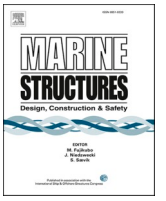

A simple rotational spring model for laterally loaded rigid piles in sand

H. Wang [a,*], B.M. Lehane [b], M.F. Bransby [c], A. Askarinejad [a], L.Z. Wang [d], Y. Hong [d]

[a] Faculty of Civil Engineering and Geosciences, Delft University of Technology, the Netherlands
[b] Department of Civil, Environmental and Mining Engineering, School of Engineering, The University of Western Australia, 35 Stirling Highway, Crawley, Perth, WA, 6009, Australia
[c] Centre for Offshore Foundation Systems, Oceans Graduate School, The University of Western Australia, 35 Stirling Highway, Crawley, Perth, WA, 6009, Australia
[d] College of Civil Engineering and Architecture, Zhejiang University, Hangzhou, China

ARTICLE INFO

Keywords:
Rigid pile
Sands
Lateral load
Hypoplastic
Pile-soil interaction

ABSTRACT

Monopiles are the most popular foundation for offshore wind turbines. These foundations typically have a low length to diameter ratio and undergo a rigid body rotation when subjected to lateral load. This paper presents results from an extensive numerical investigation involving 3D finite element analyses to demonstrate that the lateral moment-rotation response of a monopile in sand can be represented using a single non-linear rotational spring located at a depth of about 0.75 times the pile embedment. Expressions for the elastic rotational stiffness of a monopile under very low rotations are developed and these combined with observations from measured non-linear variations of rotational stiffness, that are supported by the numerical analyses, are used to develop a simple approximate expression that can be used to determine the response of a monopile to a monotonic lateral load in sand.

1. Introduction

Monopiles are the preferred foundation type for offshore wind turbines (OWTs) and have been used in more than 80% of installations in Europe [1]. The loads applied to OWTs in typical water depths up to 40 m can be resisted efficiently using large diameter (D) monopiles, where D varies between about 3 m and 10 m [2,3]. The pile lengths (L) are such that the aspect ratios (L/D) are low, typically ranging from about 2 to 8, with the consequence that the piles demonstrate rigid behaviour under combined lateral and moment loading.

The *p-y* load transfer method is the most widely used approach for the design of laterally loaded piles [4]. In this method, the monopile is modelled by a series of beam elements while the soil is represented by a series of non-interacting, non-linear springs distributed along the pile (e.g. Refs. [5,6]. However, the *p-y* method was originally proposed for small diameter piles (i.e. $D < 1$ m, $L/D > 20$), which bend in response to lateral load and experience almost zero lateral movement below a certain depth. In contrast, large diameter stubby monopiles undergo rigid body rotation when loaded laterally [7,8]. Physical experiments [9–11] and numerical studies [12,13] suggest that the API [4] *p-y* curves established for small diameter flexible piles are not applicable to large diameter rigid

* Corresponding author.
E-mail addresses: H.Wang-16@tudelft.nl (H. Wang), barry.lehane@uwa.edu.au (B.M. Lehane), fraser.bransby@uwa.edu.au (M.F. Bransby), A.Askarinejad@tudelft.nl (A. Askarinejad), wanglz@zju.edu.cn (L.Z. Wang), yi_hong@zju.edu.cn (Y. Hong).

https://doi.org/10.1016/j.marstruc.2022.103225
Received 18 August 2021; Received in revised form 19 January 2022; Accepted 6 March 2022
Available online 16 April 2022

piles. Byrne et al. [14] contest that the API *p-y* curves do not account for the significant additional resistance provided by shaft friction and base resistance and, based on findings from a joint industry project, proposed a new four-spring model for monopiles in sand, which included these resistance components [15,16]. Although the four-spring model can capture the pile-soil interaction more accurately compared with the single spring *p-y* method, the additional springs also bring extra uncertainty and complexity since each of these springs needs to be calibrated.

Wang et al. [17] performed a series of numerical analyses in a uniform sand with relative density of $D_r = 65\%$ for large diameter rigid monopiles with diameters ranging from 4 m to 10 m, but the same embedded length of 30 m. These results showed that the inaccuracies found when applying the flexible pile *p-y* model to rigid piles arise because of the unique rigid rotation failure mechanism, as shown in Fig. 1.

For such a rigid rotation mechanism, it was found that the profiles of ultimate lateral soil pressure (i.e. $P_u = p_u/D$) for different diameter piles in a uniform sand converge at the same rotation and are well represented by the simplified model of pile-soil interaction summarized in Fig. 2 [18,19]. The computed position of the rotation centre under different loading eccentricities (around 0.7–0.8*L* below the ground surface) was also found to be closely comparable to that obtained from the simplified model (Fig. 2). This model leads to the following expressions for ultimate lateral capacity (H_{ult}) and ultimate moment capacity (M_{ult}), where γ' is the effective soil unit weight, K_{P_u} is the ultimate net pressure coefficient ($=P_u/\sigma'_v$), and d is the depth of the rotation centre:

$$H_{ult} = \left(d^2 - \frac{1}{2}L^2\right)K_{P_u}D\gamma' = \left((d/L)^2 - \frac{1}{2}\right)K_{P_u}DL^2\gamma' \tag{1}$$

$$M_{ult} = H_{ult}e = \frac{\left(L^3 - 2d^3\right)K_{P_u}D\gamma'}{3} = \frac{\left(1 - 2(d/L)^3\right)K_{P_u}DL^3\gamma'}{3} \tag{2}$$

Wang et al. [17] also showed that, for the hypoplastic model employed to represent medium dense sand, the calculated lateral forces (H) and moments (M) at the mudline at a given pile rotation (θ) vary in proportion to their ultimate values. Consequently, it was found that computations for all pile diameters, at a given θ, could be unified by normalizing H by [$DL^2\,\gamma$'] and M by [$DL^3\,\gamma$']. This is illustrated for the normalized mudline moment ($M = He$) on Fig. 3, showing a unique $M/DL^3\,\gamma'$ *vs.* θ response for the analyses conducted. The uniqueness implies that the net pressure coefficient (K) given by P/σ'_v at any θ is constant.

Motivated by the consistency indicated on Fig. 3b, this paper first extends the scope of the finite element (FE) study presented in Wang et al. [17] to cover sands, under drained loading conditions, of different relative densities and piles with different lengths and loading eccentricities. The FE analyses are described and the new results are used to demonstrate the potential of a simple rotational spring model to approximate the moment-rotation response of rigid monopiles. The proposed model possesses both the simplicity of the *p-y* method (i.e. only one rotational spring is needed) and the accuracy of the four-spring model (i.e. the rigid rotation mechanism of rigid pile is the intrinsic feature of the model). FE analyses are also presented to confirm that the shear modulus of the sand controls the response and to derive a relationship between the monopile's elastic (low strain) rotational stiffness and the small strain in situ shear modulus (G_0). Supported by the findings from these analyses, the paper then uses reported field test results to deduce a simple

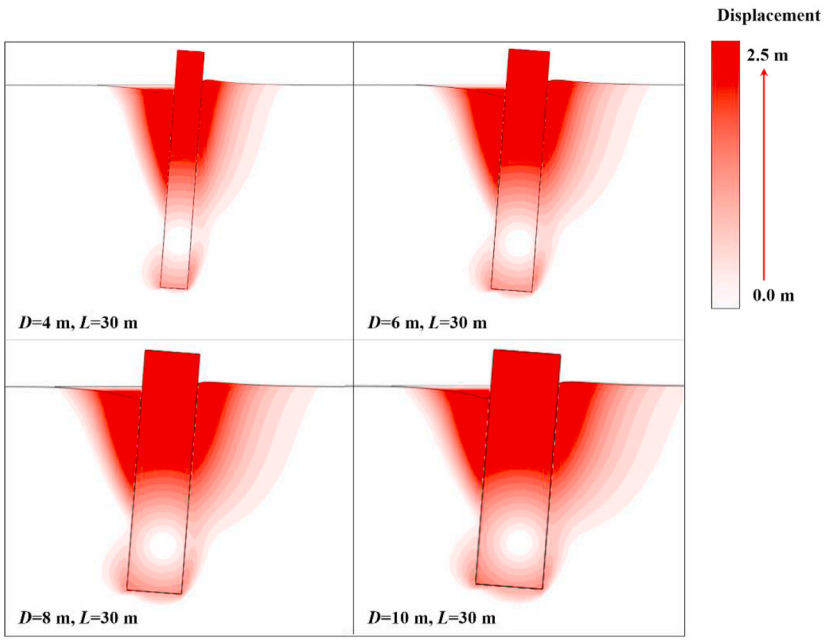

Fig. 1. Failure modes of different diameter rigid monopiles from Wang et al. [17].

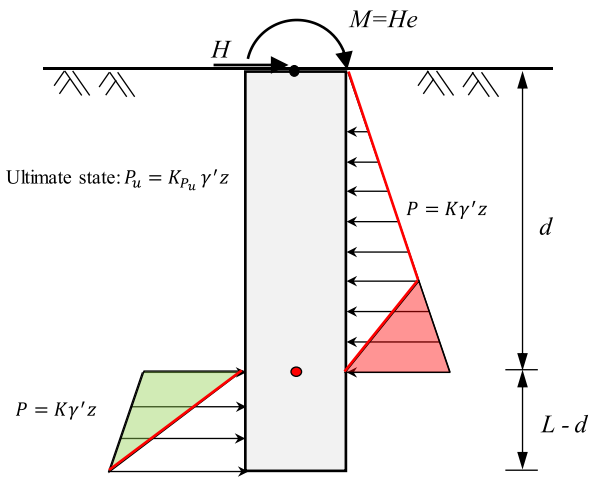

Fig. 2. Simplified model of soil-pile interaction mechanism for a laterally loaded rigid monopile (Note: the associated force and moment relative to the rotation centre of the shaded triangles are approximately equal).

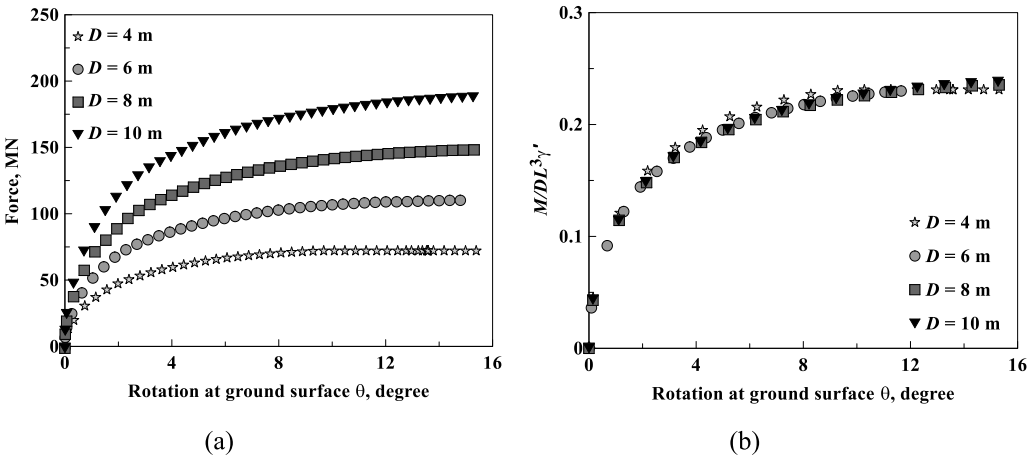

Fig. 3. Predicted lateral response of different diameter 30 m long rigid monopiles with a load eccentricity of 5 m in sand with $D_r = 65\%$: (a) load-rotation curve; (b) normalized mudline moment-rotation curve [17].

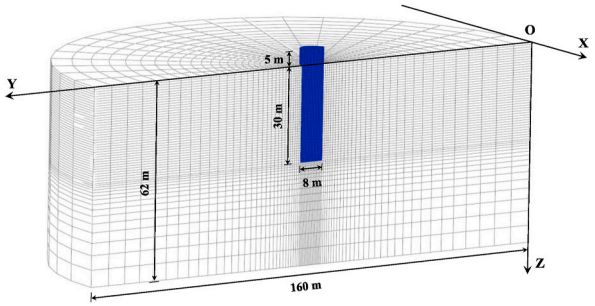

Fig. 4. A typical finite element model mesh of the 8 m diameter (D) pile with an embedded depth (L) of 30 m and loading height (e) of 5 m.

formulation for the non-linear moment-rotation response of a monopile that can be applied easily in preliminary soil-structure interaction analyses.

2. Finite element modelling

The Abaqus FE program [20] was used to perform the laterally loaded monopile analyses. The FE mesh shown in Fig. 4 of the monopile with $D = 8$ m, $L = 30$ m and $e = 5$ m (see Table 1) contains 41,515 brick elements and is typical of the meshes employed in all analyses. Considering the symmetry of the problem, only half of the pile-soil system was modelled. The domain has a diameter of $20D$ and sand extends to a depth of $4D$ beneath the tip of each pile. Radial displacements on the vertical boundaries of the domain were prevented and the bottom plane was fully fixed. Eight-node linear strain brick elements (i.e. 'C3D8' in Abaqus terminology) were used to simulate both the sand and pile. Additional simulations that involved doubling the mesh density and geometric dimensions showed a difference of less than 3% for the computed load-deflection response. The model pile was assumed to be 'wished-in-place' and fully rigid. The Coulomb model was used to simulate the interface behaviour between the pile and soil, where the tangential stress is proportional to the normal effective stress. A friction coefficient equal to two thirds of the sand friction angle was adopted in all analyses [21,22].

The hypoplastic model with intergranular strain was used to simulate the nonlinear response of the sand [23,24]. The hypoplastic model was originally proposed by Kolymbas [25] and has been improved further by many researchers to capture the stress and state dependency, strain-dependence of stiffness and stress history effects (e.g. [23,24,26,27]).

In the hypoplastic model, the relationship between stress rate and the strain rate is characterized by the following formulation:

$$\dot{\sigma} = f_b f_e [\boldsymbol{L}(\boldsymbol{\sigma}, e) : \dot{\boldsymbol{\varepsilon}} + f_d \boldsymbol{N}(\boldsymbol{\sigma}, e)\dot{\boldsymbol{\varepsilon}}] \tag{3}$$

where $\dot{\boldsymbol{\sigma}}$ is a stress rate tensor, $\dot{\boldsymbol{\varepsilon}}$ is a strain rate tensor, $\boldsymbol{L}$ is a fourth order tensor, $\boldsymbol{N}$ is a second-order tensor, f_b is a barotropy factor reflecting the influence of soil state, f_d and f_e are pyknotropy factors reflecting the influence of relative density. The model has eight basic material parameters (i.e. $\varphi_c^{'}$, h_s, n, e_{d0}, e_{i0}, e_{c0}, α, β) for modelling nonlinear and state dependent response and additional five parameters accounting for strain- and stress-dependent stiffness at small strains (i.e. m_R, m_T, R, β_r, χ). Details about the model can be found in von Wolffersdorff [23] and Niemunis & Herle [24]. The constitutive model is implemented in Abaqus by a user-defined subroutine [28].

The model parameters for Toyoura sand calibrated against the stress-path controlled triaxial tests by Hong et al. [21] and validated against the centrifuge tests of laterally loaded piles by Wang et al. [17] are adopted in this study (as summarized in Table 1). Parameters for Toyoura sand were used because the numerical approach could be validated against experimental pile test data available for this sand. The mechanical response of Toyoura sand is also typical of a clean silica sand.

A summary of the FE analyses performed is provided in Table 2 and comprised 128 simulations in addition to the 28 simulations described in Wang et al. [17]. These simulations examined the monotonic lateral response of monopiles with different diameters (D = 4, 6, 8 and 10 m) and embedded lengths (L = 20, 30 and 40 m) under a wide range of loading eccentricities (e = 5, 10, 20, 40, 60, 80, 100 m) and in different relative density sands (D_r = 20%, 30%, 40%, 50%, 65%, 70% and 80%).

3. Rotational spring model

All the FE analyses showed that a change in the loading eccentricity (e) led to small changes in the depth of the rotation centre (d) (as defined in Fig. 2), where d reduced as e increased. An illustration of the slight sensitivity of d to e is provided on Fig. 5 for the case of 30 m long piles in sand with relative densities (D_r) of 40%, 65% and 80% at ultimate conditions. It is evident that the average value of d of $0.75L$ (where L is the embedded length) is within about 3% of all computed values. Fig. 5 also plots the variation of d with e predicted using the simplified pressure distribution shown on Fig. 2. This variation is closely comparable to the Abaqus predictions

Table 1
Calibrated parameters of the hypoplastic model for Toyoura sand [21].

	Description	Parameter	Values
Basic hypoplastic model [23]	Effective angle of shearing resistance at critical state	$\varphi_c^{'}$	31
	Hardness of granulates (kPa)	h_s	2.6×10^6
	Exponent in the power law for proportional compression	n	0.27
	Minimum void ratio at zero pressure	e_{d0}	0.61
	Maximum void ratio at zero pressure	e_{i0}	0.98
	Critical void ratio at zero pressure	e_{c0}	1.1
	Exponent	α	0.11
	Exponent	β	4
Intergranular strain concept [24]	Parameter controlling initial shear modulus upon 180° strain path reversal	m_R	8
	Parameter controlling initial shear modulus upon 90°strain path reversal	m_T	4
	Size of elastic range	R	2×10^{-5}
	Parameter controlling degradation rate of stiffness with strain	β_r	0.15
	Parameter controlling degradation rate of stiffness with strain	χ	1.0
Initial state	Relative density of sand	D_r	20–80%

Table 2
Dimensions of the piles, loading conditions and soil densities modelled in the numerical simulations [2,14].

Note	Relative density (D_r)	Diameter (D)	Embedded Length (L)	Loading eccentricity (e)
Numerical parametric study [17]	65%	4, 6, 8, 10 m	30 m	5, 10, 20, 40, 60, 80, 100 m
Numerical parametric study (This study)	65%	4, 6, 8, 10 m	20 m	5, 10, 20, 40, 60, 80, 100 m
	65%	4, 6, 8, 10 m	40 m	5, 10, 20, 40, 60, 80, 100 m
	40%	4, 6, 8, 10 m	30 m	5, 10, 20, 40, 60, 80, 100 m
	80%	4, 6, 8, 10 m	30 m	5, 10, 20, 40, 60, 80, 100 m
	20%	4, 6, 8, 10 m	30 m	5 m
	30%	4, 6, 8, 10 m	30 m	5 m
	50%	4, 6, 8, 10 m	30 m	5 m
	70%	4, 6, 8, 10 m	30 m	5 m

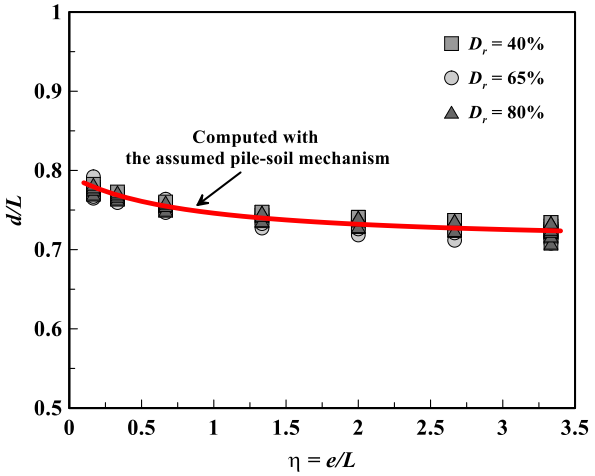

Fig. 5. Rotation centre position computed from FE simulations (D_r = 40, 65, 80%, D = 4, 6, 8, 10 m, L = 30 m) and the simplified pressure distribution.

confirming the applicability of the simplified pressure distribution and showing that adoption of a constant d value of 0.75L is reasonable at any pile rotation provided that the soil pressure distribution is of a similar form (i.e. the pressure coefficient, K, and hence the sand relative density is constant).

On the basis of these observations, the response of a laterally loaded rigid pile can be simplified to that of a beam hinged at a rotation centre at a depth of 0.75L and constrained by a rotational spring, as shown in Fig. 6. If the overall lateral response of a rigid pile is represented by this rotational spring, a change of force and moment at different loading eccentricities is simply a result of a change in the loading arm relative to the rotation centre. The lateral response of a rigid pile under different loading eccentricities can therefore be unified by presenting the results in terms of moment relative to the rotation centre, where the moment is $M_R = H\ (e + 0.75L)$.

The validity of a single non-linear rotational spring located at a depth of 0.75L is assessed in Fig. 7 which presents typical FE results for (a) piles with embedded lengths of 20 m, 30 m and 40 m in medium dense sand and (b) piles in sands with different relative densities (D_r) but a fixed length (of 30 m). The applied moments about the rotation centre (at a depth of 0.75L) are normalized by

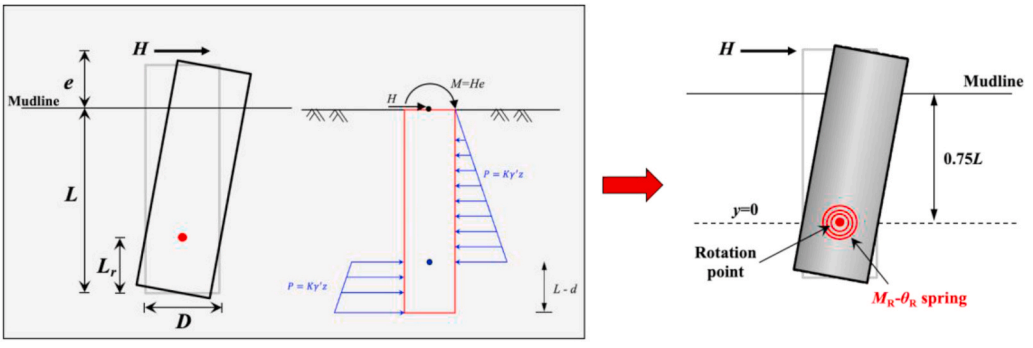

Fig. 6. Simplified pressure distribution and corresponding single rotational spring.

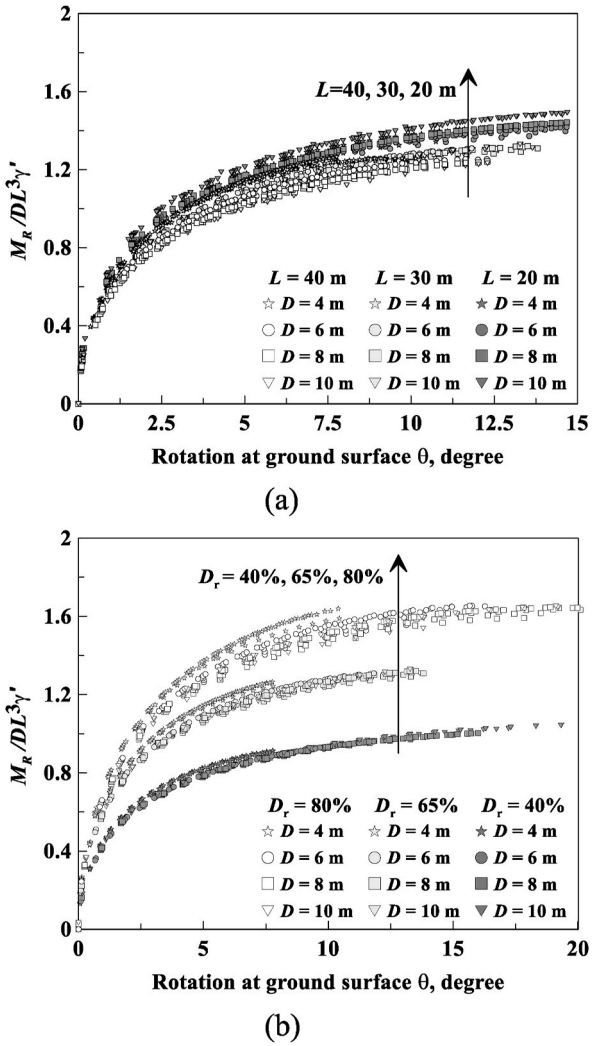

Fig. 7. Abaqus predictions for rotational spring for (a) L = 20, 30, 40 m (D_r = 65%, D = 4–10 m, e = 5–100 m) and (b) D_r = 40, 65, 80% (D = 4–10 m, e = 5–100 m, L = 30 m).

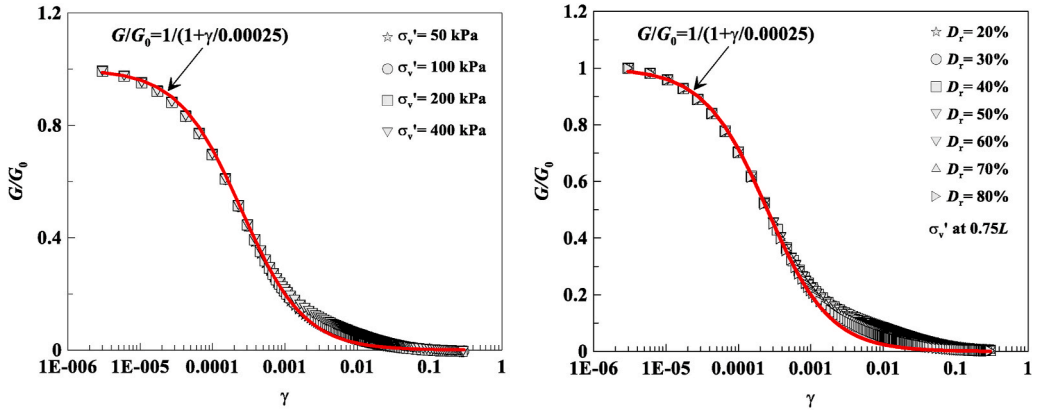

Fig. 8. Shear modulus degradation curves from DSS simulations (Note: the σ'_v in Fig. 7b is the stress at 0.75L).

[$DL^3\gamma'$], as in Fig. 3b.

It is clear that, at a given D_r, there is a virtually unique relationship between normalized moment [$M_R/(DL^3\gamma')$] and pile rotation (θ). A slight reduction in the normalized moment at a given rotation is evident as the pile length increases at a higher level of capacity mobilisation (Fig. 7a); this may be attributed to reduced sand dilatancy for the average higher stress levels operational for longer piles [29]. As anticipated, the rotational moment capacity increases with D_r (Fig. 7b), approximately doubling as D_r increases from 40% to 80%.

4. Relationship between the rotational spring and shear stiffness of sand

Having identified that there is likely to be a unique M_R-θ curve for a given pile size and sand relative density, it is necessary to establish the elemental sand characteristics that control the shape of this curve to provide support for the simple formulation presented later. The rotational stiffness, K_θ, is defined here as the secant value (M_R/θ), which has a maximum (elastic) value of $K_{\theta\_initial}$ at very low pile rotations.

4.1. Relationship with elemental secant shear modulus

Computed variations of normalized secant shear stiffness (G/G_0) with shear strain (γ) for elements of Toyoura sand with the hypoplastic model parameters given in Table 1 subjected to direct simple shear (DSS) are plotted on Fig. 8. Detailed comparisons between predictions and laboratory element tests are provided by Hong et al. [21]. The variations of G/G_0 with strain do not exhibit a significant dependence on D_r and σ'_v at low to intermediate strains. It was found that the computed shear modulus degradation curves in Fig. 8 can be approximated by the following hyperbolic function:

$$G / G_0 = 1 / (1 + \gamma / 0.00025) \tag{4}$$

The corresponding calculated variations of normalized secant rotational stiffness ($K_\theta/K_{\theta\_initial}$) with rotation (θ) for all the simulations in this study are presented in Fig. 9. This figure also plots the following best fit hyperbolic curve to the computed variations:

$$K_\theta / K_{\theta\_initial} = 1/(1 + \theta/0.00025) \tag{5}$$

The form of Equation (5) is identical to Equation (4) and strongly suggests direct correspondence between the rotational stiffness and the elemental shear modulus; the observed equivalence indicates that the average operational shear strain is equal to the pile rotation for this constitutive model. Analogous correspondence between soil at element scale and foundation response at full scale has been deduced by Atkinson [30] for prediction of (non-linear) settlement of shallow foundations and by Johansson et al. [31] for predictions of rocking stiffness of shallow foundations. Similarly, Bransby [32] and Zhang & Andersen [33] showed that the load transfer curves of laterally loaded piles can be scaled from the non-linear stress-strain curves of soil. Although limitations of the hypoplastic model may mean that Equation (5) is not directly applicable to field data (which is examined below), the analyses demonstrate the key importance of the in-situ shear modulus to estimation of a monopile's response.

4.2. Relationship with small strain shear modulus

Given the clear importance of the sand shear stiffness, the relationship between the initial rotational stiffness ($K_{\theta\_initial}$) and the small strain elemental shear modulus (G_0) was investigated in a series of 3D FE simulations in elastic soils. Over 500 FE analyses were

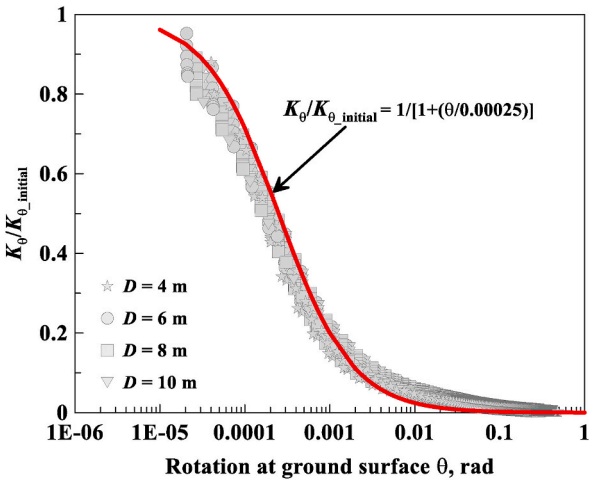

Fig. 9. Normalized secant stiffness degradation curves of rotational springs.

performed on rigid piles with different diameters ($D = 4, 6, 8, 10$ m) and embedded lengths ($L = 10, 20, 30, 40$ m) for a range of loading eccentricities ($e = 1, 5, 10, 20, 40, 80$ m). Three different profiles of G_0 were considered: (a) G_0 constant with depth; (b) G_0 increasing linearly with depth and (c) G_0 increasing with the square root of depth. For each pile in each soil, both a fully rough interface and a semi-rough interface (with an interface friction angle of around 21°) were examined.

Statistical analyses of the computations indicated that a suitable format for $K_{\theta\_initial}$ was as follows [consistent with the equation for rotational stiffness of rigid foundation in Shadlou & Bhattacharya [34]]:

$$K_{\theta\_initial} = C_k\, DL^2\, G_{0.75L} \tag{6}$$

where $G_{0.75L}$ is the reference in situ G_0 value at the rotation point and C_k is a coefficient that varies primarily with L/D and the form of the G_0 profile. All computed results are plotted on Fig. 10 where the dominant effect of L/D and the form of the G_0 profile is demonstrated. Almost identical C_k values were evaluated for the two interface conditions considered. The following equation with fitting parameters *a, b, c* and *d* is shown on Fig. 10 to provide a good representation of C_k values for the three selected G_0 profiles.

$$C_k = \left[a \times e^{b\times\frac{L}{D}} + c \times e^{d\times\frac{L}{D}}\right] \; for\; 10 \geq \frac{L}{D} \geq 1, where \tag{7}$$

$a = 9.1$, $b = -2.24$, $c = 2.71$ and $d = 0.065$ when G_0 is constant with depth
$a = 6.5$, $b = -1.5$, $c = 1.4$ and $d = 0.044$ when G_0 increases linearly with depth
$a = 6.2$, $b = -1.62$, $c = 1.85$ and $d = 0.053$ when G_0 varies with the square root of depth.

G_0 of sand usually varies with the square root of the stress level and Fig. 10 indicates that $K_{\theta\_initial}$ can be taken as approximately $2.5G_{0.75L}DL^2$ for typical monopiles in uniform sand deposits. When G_0 is constant with depth, the analyses indicate $K_{\theta\_initial}$ is about $4G_{0.75L}\, DL^2$ when $L/D < 6$, which is comparable to the value recommended by Amar Bouzid [35]. It is also noted that in situ G_0 values are now easily and conveniently measured in seismic cone penetration tests.

5. Proposed rotational spring formulation

Investigation of a formulation describing the degradation of a monopile's rotational stiffness with rotation similar to that developed numerically (Eq. (5)) was conducted using available high-quality tests on laterally loaded rigid piles in reasonably uniform sands. A brief summary of the four test series considered is given in the following and in Tables 3–6, which also presents details on the pile geometries and in situ $G_{0.75L}$ values. Figs. 11–14 present the measured lateral load-displacement responses of the 25 pile tests in these experimental programmes.

5.1. Centrifuge model tests by Klinkvort and Hededal [36]

Klinkvort and Hededal [36] performed a series of centrifuge model tests at an acceleration of 75 g on piles with $L/D = 6$ in Fontainebleau sand [37] with relative density of 86–93% under different loading eccentricities ($e/L = 0.42, 1.38, 1.75, 2.13, 2.50$ and 2.88). The model piles had a prototype diameter and embedded length of 3 m and 18 m, respectively (Fig. 11). The small strain shear modulus ($G_{0.75L}$) at the pile rotation centre was calculated using the following empirical formula provided by Gaudin et al. [37] for Fontainebleau sand:

$$G_0 = 500\sqrt{p' p_a}\;\frac{1}{v_{sand}{}^{1.3}} \tag{8}$$

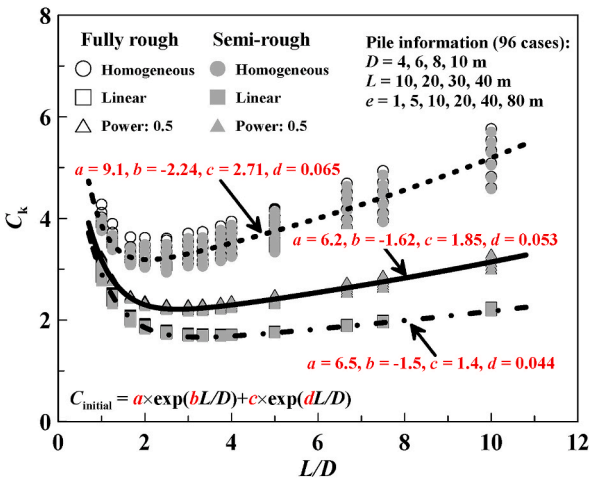

Fig. 10. Computed C_k values and predictions obtained using Eq. (7).

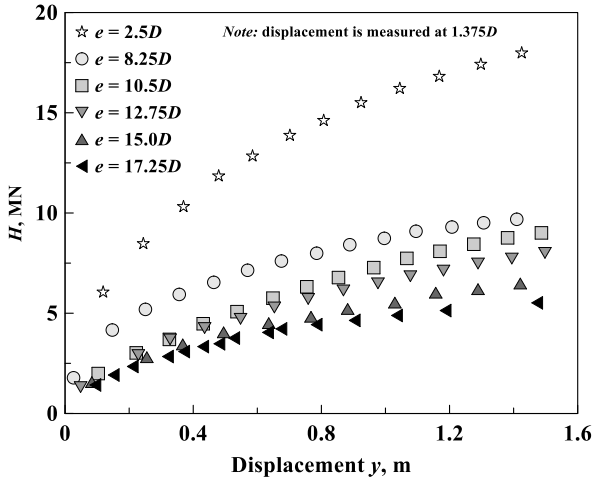

Fig. 11. Load-deflection response of centrifuge tests in Klinkvort and Hededal [36].

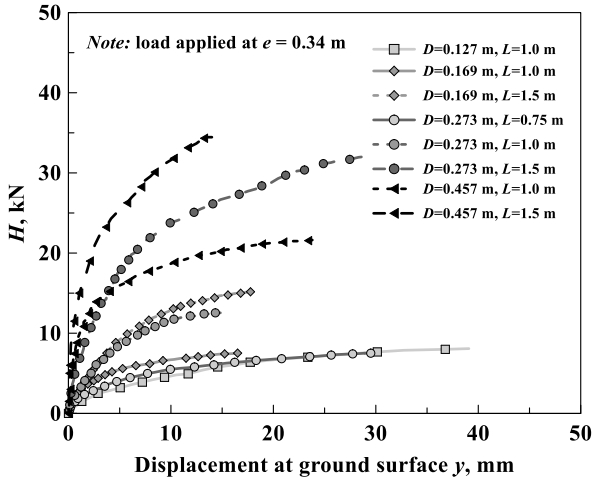

Fig. 12. Load-deflection response of field tests in Wang et al. [8].

where p' is the mean effective stress, p_a is atmospheric pressure (100 kPa) and ν_{sand} is void ratio. The $G_{0.75L}$ and corresponding $K_{\theta\_\text{initial}}$ values determined from Eq. (7) assuming G_0 varied with the square root of depth are presented in Table 3.

5.2. Field tests by Wang et al. [8]

Wang et al. [8] performed a series of small-scale field tests at the University of Western Australia's Shenton Park field test site. The soil stratigraphy comprises aeolian siliceous sand with a uniform relative density estimated from the CPTs tests of about 64%. Eight lateral load tests were conducted on piles with diameters ranging from 127 mm to 457 mm and embedded lengths between 0.75 m and 1.5 m (Fig. 12). The small strain shear moduli ($G_{0.75L}$) at the pile rotation centers was assessed from seismic cone penetration test data [38] and $K_{\theta\_\text{initial}}$ values were evaluated from Eq. (7) for a G_0 profile that varied linearly with depth.

5.3. Field tests by McAdam et al. [15]

The PISA (Pile–Soil Analysis) joint industry project [15] involved a series of large-scale field tests at Dunkirk, northern France. The sand at the site is a normally consolidated marine Pleistocene sand. The relative density in the upper 3 m is around $D_r = 100\%$ and about 75% at deeper levels. The test program employed three pile diameters ($D = 0.273$ m, 0.762 m and 2.0 m) with aspect ratios (L/D) and loading eccentricities (e/L) in the range of 2.9–8 and 0.9 to 4.5 respectively (Fig. 13). Small strain shear moduli at the pile rotation centers ($G_{0.75L}$) are provided by Zdravković et al. [39]. $K_{\theta\_\text{initial}}$ values were evaluated from Eq. (7) for a G_0 profile that varied linearly with depth. Details of the sand and piles are summarized in Table 5.

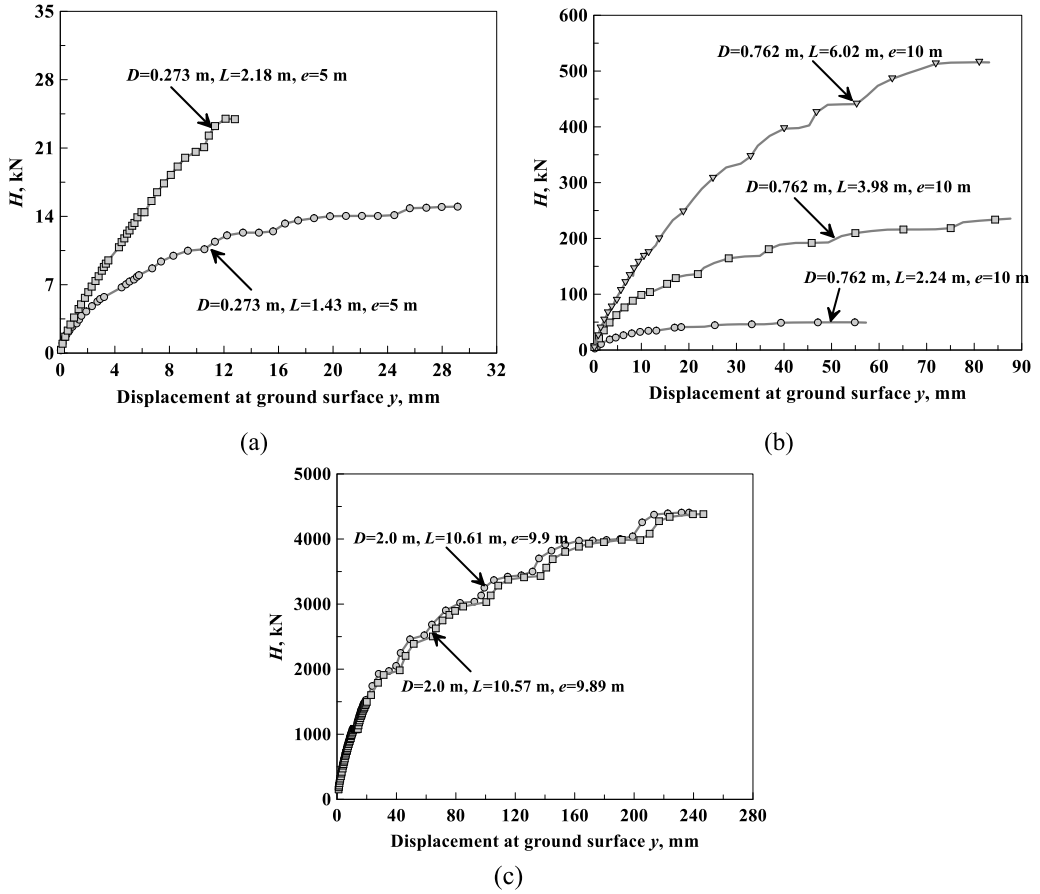

Fig. 13. Load-deflection response of field tests in McAdam et al. [15].

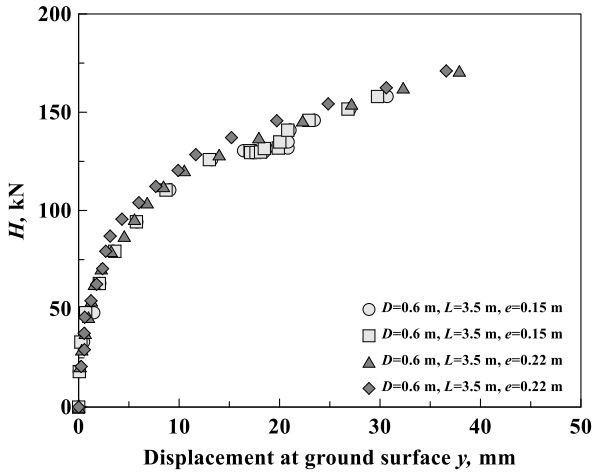

Fig. 14. Load-deflection response of field tests in Belpile (2021).

Table 3
Key features of piles and sand in tests of Klinkvort and Hededal [36].

Test No.	Test K1	Test K2	Test K3	Test K4	Test K5	Test K6
D (m)	3.0	3.0	3.0	3.0	3.0	3.0
L (m)	18.0	18.0	18.0	18.0	18.0	18.0
L/D	6	6	6	6	6	6
e/L	0.42	1.38	1.75	2.13	2.50	2.88
$G_{0.75L}$ (MPa)	114.4	111.3	115.2	110.5	110.5	109.7
$K_{\theta\_initial}$ (MNm/rad)	282,462	274,683	284,468	272,797	272,797	270,934

Table 4
Key features of piles and sand in tests of Wang et al. [8].

Test NO.	Test W1	Test W2	Test W3	Test W4	Test W5	Test W6	Test W7	Test W8
D (m)	0.127	0.169	0.169	0.273	0.273	0.273	0.457	0.457
L (m)	1.0	1.0	1.5	0.75	1.0	1.5	1.0	1.5
L/D	7.9	5.9	8.9	2.7	3.7	5.5	2.2	3.3
e/L	0.34	0.34	0.23	0.45	0.34	0.23	0.34	0.23
$G_{0.75L}$ (MPa)	60.3	60.3	70.7	51.4	60.3	70.7	60.3	70.7
$K_{\theta\_initial}$ (MNm/rad)	7.65	10.19	26.90	7.89	16.45	43.45	27.54	72.74

Table 5
Key features of piles and sand in tests of McAdam et al. [15].

Test NO.	Test M1	Test M2	Test M3	Test M4	Test M5	Test M6	Test M7
D (m)	0.273	0.273	0.762	0.762	0.762	2.0	2.0
L (m)	1.43	2.18	2.24	3.98	6.02	10.61	10.57
L/D	5.24	8	2.94	5.22	7.90	5.31	5.29
e/L	3.5	2.3	4.46	2.51	1.66	0.93	0.94
$G_{0.75L}$ (MPa)	45	48	60	83	85	101.7	101.5
$K_{\theta\_initial}$ (MNm/rad)	25.1	62.3	229.4	1001.8	2347.3	22901.8	22690.9

Table 6
Key features of piles and sand in tests of Belpile (2021).

Test NO.	Test B1	Test B2	Test B3	Test B4
D (m)	0.6	0.6	0.6	0.6
L (m)	3.5	3.5	3.5	3.5
L/D	5.83	5.83	5.83	5.83
e/L	0.043	0.043	0.063	0.063
$G_{0.75L}$ (MPa)	93.9	93.9	93.9	93.9
$K_{\theta\_initial}$ (MNm/rad)	1250	1250	1250	1250

5.4. Field tests by Belpile (2021)

Four lateral load tests were performed by Belpile (2021) on 600 mm diameter, 3.5 m long concrete continuous flight auger piles at a sand site in Perth, Australia (Fig. 14). The $G_{0.75L}$ values were determined from seismic cone penetration tests and $K_{\theta\_initial}$ values were evaluated from Eq. (7) assuming G_0 varied linearly with depth. Relevant details are summarized in Table 6.

5.5. Collation of field measured pile rotational stiffness values

The (secant) K_θ values were determined from the lateral load (H) and deflection (y) data presented in each case history from the following expression:

$$K_\theta = M_R / \theta = H(e + 0.75L) / \theta \tag{9}$$

These K_θ values are normalized by the corresponding $K_{\theta\_initial}$ values provided in Tables 3–6 and plotted against pile rotation (θ) on Fig. 15. As shown in Fig. 15a, initial examination indicated that the variation of $K_\theta/K_{\theta\_initial}$ with rotation (θ) showed significant variability, with stronger degradation of stiffness with rotation arising at low stress levels such as for the tests on the short piles plotted on Fig. 12. This trend, which is not simulated in the hypoplastic model (see Fig. 8a), is consistent with the tendency for the shear stiffness of sand to degrade more rapidly with shear strain at lower stress levels [40]. Stokoe et al. [41] model this stress level dependency by defining a reference strain when the secant stiffness is half of the small strain stiffness and found data over a wide range of

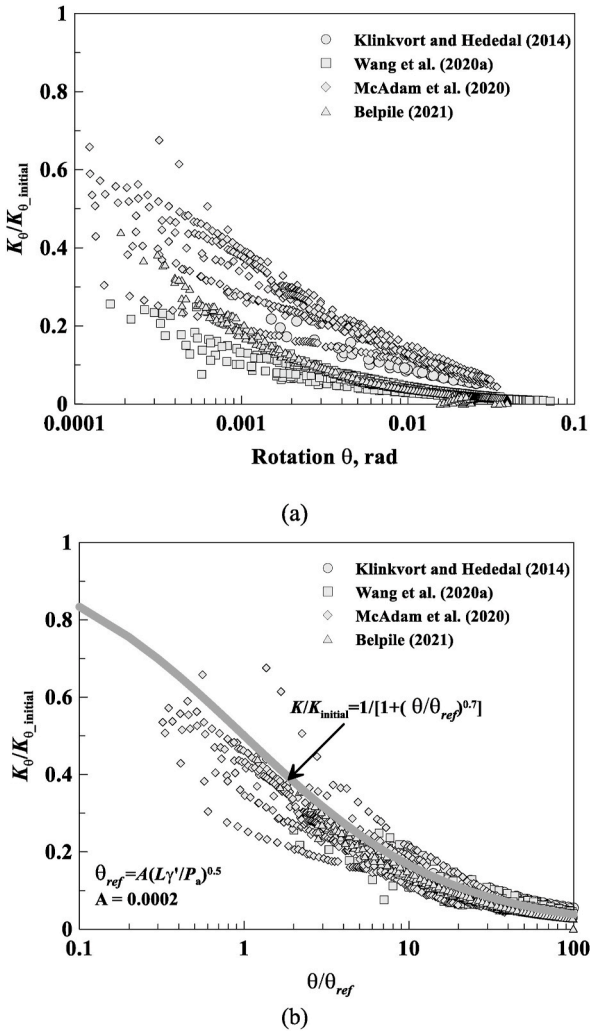

Fig. 15. $K_\theta/K_{\theta\_initial}$ *vs.* θ and/θ_{ref} for 25 pile tests at four sand sites (a) $K_\theta/K_{\theta\_initial}$ *vs.* θ; (b) $K_\theta/K_{\theta\_initial}$ *vs.* θ/θ_{ref}.

stress levels were unified when this reference strain was assumed proportional to the square root of the stress level. In addition, Fahey & Carter [42] found that in situ shear stiffness degradation curves are often better described using a modified hyperbolic format [and not the hyperbolic format deduced from the hypoplastic model in Eq. (5)]. Based on these observations, the following best-fit formulation was derived for the database of 25 lateral pile tests:

$$K_\theta \Big/ K_{\theta\_initial} = 1 \Big/ \left[1 + \left(\theta/\theta_{ref}\right)^{0.7}\right] \tag{10a}$$

$$where \quad \theta_{ref} = 0.0002 \times \left(\gamma' L/p_{ref}\right)^{0.5}, \tag{10b}$$

where $p_{ref} = 100\ kPa$ and γ' is effective soil unit weight.

Fig. 15b shows the result of combining Equation (10) with Equation (7). The new relationships provide a good representation of the response of 25 rigid monopiles with a wide range of diameters and load eccentricities in four different sand deposits.

Equation (10) combined with Equation (7) provide a simple and practical means of modelling the non-linear moment-rotation response of a monopile that is anchored to field data and can be applied simply in preliminary soil-structure interaction analyses. The advantage of the method is that it does not require definition of multiple lateral, distributed moment and pile base springs to achieve an acceptable solution, but encapsulates the overall rotational mechanism in a single spring (which varies with pile aspect ratio and typical profiles of G_o). The approach could be refined further by linking the $K_\theta/K_{\theta\_initial}$ degradation curve with the soil stress-strain curve directly (as attempted for *p-y* curves by Bransby [43]; Zhang and Andersen [33]; etc.) or by incorporating the effect of layered soils. However, current detailed design practice involves the use of three-dimensional FE analysis using tuned site-specific soil parameters and advanced constitutive models which will thereby incorporate these effects directly.

6. Conclusions

A series of 3D FE numerical analyses of laterally loaded piles in uniform sand, simulated using the hypoplastic model, has shown that the lateral response of a rigid pile can be represented well as a single non-linear rotational spring (K_θ) located at a depth of about 0.75 times the pile embedment. These analyses have also demonstrated that the non-linearity of the spring is related directly to the non-linearity of the shear stiffness of the sand. The FE analyses are used to establish a relationship between the rotational spring stiffness at very low pile rotations ($K_{\theta\_initial}$) and the in situ small strain shear modulus (G_0). This relationship is combined with field measurements of the variation of K_θ with θ to deduce a simple expression for K_θ that is consistent with the numerical analyses performed. The relationship provides designers with a rapid means of determining the approximate response of a monopile to lateral load in uniform, drained sand.

Declaration of competing interest

The authors declare that they have no known competing financial interests or personal relationships that could have appeared to influence the work reported in this paper.

Acknowledgements

The authors gratefully acknowledge the financial supports provided by National Key Research and Development Program (2018YFE0109500), National Natural Science Foundation of China (51779221, 51909249 and 51939010) and Zhejiang Provincial Natural Science Foundation (LHZ20E090001, LQ19E090001). The third author is the Fugro Chair in Geotechnics, whose support is gratefully acknowledged.

References

[1] Ramírez L, Fraile D, Brindley G. Offshore wind in Europe: key trends and statistics 2020. 2021.
[2] Negro V, López-Gutiérrez JS, Esteban MD, Alberdi P, Imaz M, Serraclara JM. Monopiles in offshore wind: preliminary estimate of main dimensions. Ocean Eng 2017;133:253–61.
[3] Li Q, Prendergast LJ, Askarinejad A, Chortis G, Gavin K. Centrifuge modeling of the impact of local and global scour erosion on the monotonic lateral response of a monopile in sand. Geotech Test J 2020;43(5).
[4] API (American Petroleum Institute). Geotechnical and foundation design considerations. Washington, DC: API; 2011. API RP 2GEO.
[5] Reese LC, Cox WR, Koop FD. Analysis of laterally loaded piles in sand. Offshore technology in civil engineering Hall of fame papers from the early years. 1974. p. 95–105.
[6] Doherty P, Gavin K. Laterally loaded monopile design for offshore wind farms. Proceedings of the Institution of Civil Engineers-Energy 2012;165(1):7–17.
[7] Hong Y, He B, Wang LZ, Wang Z, Ng CWW, Mašín D. Cyclic lateral response and failure mechanisms of semi-rigid pile in soft clay: centrifuge tests and numerical modelling. Can Geotech J 2017;54(6):806–24.
[8] Wang H, Lehane BM, Bransby MF, Wang LZ, Hong Y. A simple approach for predicting the ultimate lateral capacity of a rigid pile in sand. Géotech Lett 2020;10(3):429–35.
[9] Klinkvort RT. Centrifuge modelling of drained lateral pile - soil response: application for offshore wind turbine support structures. PhD Thesis. Technical University of Denmark; 2012.
[10] Choo YW, Kim D. Experimental development of the *p-y* relationship for large-diameter offshore monopiles in sands: centrifuge tests. J Geotech Geoenviron Eng 2015;142(1):04015058.
[11] Qi WG, Gao FP, Randolph MF, Lehane BM. Scour effects on *p-y* curves for shallowly embedded piles in sand. Geotechnique 2016;66(8):648–60.
[12] Thieken K, Achmus M, Lemke K. A new static *p-y* approach for piles with arbitrary dimensions in sand. Geotechnik 2015;38(4):267–88.
[13] Wang H, Wang LZ, Hong Y, He B, Zhu RH. Quantifying the influence of pile diameter on the load transfer curves of laterally loaded monopile in sand. Appl Ocean Res 2020;101:102196.
[14] Byrne BW, Mcadam R, Burd HJ, Houlsby GT, Martin CM, Zdravkovic L, Taborda DMG, Potts DM, Jardine RJ, Sideri M, Schroeder FC, Gavin K, Doherty P, Igoe D, Muir Wood A, Kallehave D, Skov Gretlund J. New design methods for large diameter piles under lateral loading for offshore wind applications. In: 3rd international symposium on frontiers in offshore Geotechnics - ISFOG; 2015. p. 705–10. Oslo, Norway.
[15] McAdam RA, Byrne BW, Houlsby GT, Beuckelaers WJ, Burd HJ, Gavin KG, Potts DM. Monotonic laterally loaded pile testing in a dense marine sand at Dunkirk. Geotechnique 2020;70(11):986–98.
[16] Burd HJ, Taborda DM, Zdravković L, Abadie CN, Byrne BW, Houlsby GT, McAdam RA. PISA design model for monopiles for offshore wind turbines: application to a marine sand. Géotechnique; 2020. p. 1–19.
[17] Wang H, Bransby MF, Lehane BM, Wang LZ, Hong Y. Numerical investigation of the monotonic drained lateral behaviour of large diameter rigid piles in medium dense uniform sand. Géotechnique; 2021. p. 1–39.
[18] Petrasovits G, Award A. Ultimate lateral resistance of a rigid pile in cohesionless soil. In: Proceedings of 5th European conference on soil mechanics and foundation engineering, madrid, vol. 3; 1972. p. 407–12.
[19] LeBlanc C, Houlsby GT, Byrne BW. Response of stiff piles in sand to long-term cyclic lateral loading. Geotechnique 2010;60(2):79–90.
[20] Systèmes Dassault. ABAQUS 6.8 analysis user's manual. Providence, RI: Simulia Corp; 2007.
[21] Hong Y, Koo CH, Zhou C, Ng CW, Wang LZ. Small strain path-dependent stiffness of Toyoura sand: laboratory measurement and numerical implementation. Int J GeoMech 2016;17(1):04016036.
[22] Achmus M, Schmoor KA, Herwig V, Matlock B. Lateral bearing behaviour of vibro-and impact-driven large-diameter piles in dense sand. Geotechnik 2020;43(3):147–59.
[23] Von Wolffersdorff PA. A hypoplastic relation for granular materials with a predefined limit state surface. Mech Cohesive-Frict Mater 1996;1(3):251–71.
[24] Niemunis A, Herle I. Hypoplastic model for cohesionless soils with elastic strain range. Mech Cohesive-Frict Mater 1997;2(4):279–99.
[25] Oztoprak S, Bolton MD. Stiffness of sands through a laboratory test database. Geotechnique 2013;63(1):54–70.
[26] Wu W, Bauer E. A simple hypoplastic constitutive model for sand. Int. J. Numer. Anal. Methods GeoMech. 1994;18(12):833–62.
[27] Wu W, Bauer E, Kolymbas D. Hypoplastic constitutive model with critical state for granular materials. Mech. Mater. 1996;23(1):45–69.
[28] Gudehus G, Amorosi A, Gens A, Herle I, Kolymbas D, Mašín D, Muir Wood D, Niemunis A, Nova R, Pastor M. The soilmodels. info project. Int J Numer Anal Methods GeoMech 2008;32(12):1571–2.
[29] Richards IA, Bransby MF, Byrne BW, Gaudin C, Houlsby GT. Effect of stress level on response of model monopile to cyclic lateral loading in sand. J Geotech Geoenviron Eng 2021;147(3):04021002.

[30] Atkinson JH. Non-linear soil stiffness in routine design. Geotechnique 2000;50(5):487–508.
[31] Johansson J, Sivasithamparam N, Zhang YH, Engin HK. Simple method for computing nonlinear foundation rocking stiffness and damping. In: 4th international symposium on frontiers in offshore Geotechnics. American Society of Civil Engineers; 2020. p. 1824–33.
[32] Bransby MF. Selection of *p–y* curves for the design of single laterally loaded piles. Int J Numer Anal Methods GeoMech 1999;23(15):1909–26.
[33] Zhang Y, Andersen KH. Scaling of lateral pile *p-y* response in clay from laboratory stress-strain curves. Mar Struct 2017;53:124–35.
[34] Shadlou M, Bhattacharya S. Dynamic stiffness of monopiles supporting offshore wind turbine generators. Soil Dynam Earthq Eng 2016;88:15–32.
[35] Amar Bouzid D. Numerical investigation of large-diameter monopiles in sands: critical review and evaluation of both API and newly proposed *p-y* curves. Int J GeoMech 2018;18(11):04018141.
[36] Klinkvort RT, Hededal O. Effect of load eccentricity and stress level on monopile support for offshore wind turbines. Can Geotech J 2014;51(9):966–74.
[37] Gaudin C, Schnaid F, Garnier J. Sand characterization by combined centrifuge and laboratory tests. Int J Phys Model Geotech 2005;5(1):42–56.
[38] Schneider JA. Analysis of piezocone data for displacement pile. Ph.D. Thesis. University of Western Australia; 2007.
[39] Zdravković L, Jardine RJ, Taborda DM, Abadias D, Burd HJ, Byrne BW, Ushev E. Ground characterisation for PISA pile testing and analysis. Geotechnique 2020; 70(11):945–60.
[40] Ishibashi I, Zhang X. Unified dynamic shear moduli and damping ratios of sand and clay. Soils Found 1993;33(1):182–91.
[41] Stokoe KH, Hwang SK, Darendeli MB, Lee NJ. Correlation study of nonlinear dynamic soils properties. Aiken, SC. Westinghouse Savannah River Company; 1995.
[42] Fahey M, Carter JP. A finite element study of the pressuremeter test in sand using a nonlinear elastic plastic model. Can Geotech J 1993;30(2):348–62.
[43] Bransby MF. Selection of *p-y* curves for the design of single laterally loaded piles. Int J Numer Anal Methods GeoMech 1999;23(15):1909–26.